Int. J. Heat Mass Transfer. Vol. 29, No. 8, pp. 1227–1235, 1986
Printed in Great Britain

0017–9310/86 $3.00 + 0.00
Pergamon Journals Ltd.

Streamwise distribution of the recovery factor and the local heat transfer coefficient to an impinging circular air jet

R. J. GOLDSTEIN, A. I. BEHBAHANI* and K. KIEGER HEPPELMANN†
Mechanical Engineering Department, University of Minnesota, Minneapolis, MN 55455, U.S.A.

Abstract—An investigation of the radial distribution of the recovery factor and the local heat transfer for an axisymmetric impinging air jet formed by a smooth nozzle is described. The recovery factor is dependent on the jet nozzle to impingement plate spacing, but is independent of jet Reynolds number. The maximum stagnation region heat transfer occurs at a nozzle to impingement plate spacing of about eight jet diameters. A correlation is obtained for the average heat transfer from the surface.

1. INTRODUCTION

IN MANY industrial systems—including high temperature gas turbines, paper and glass manufacturing plants and high density electrical and electronic equipment—impinging jets of fluid, usually air, are used to cool, heat or dry a surface. Over the past three decades numerous studies have been reported on the heat transfer to impinging single and multiple jets. Table 1 lists investigations [1–25] which considered a single impinging circular jet. A survey of early works is provided by Martin [26].

Gardon and Cobonpue [3] first described the rate of heat transfer to an impinging jet as proportional to the difference between the (impingement) plate temperature and the adiabatic wall temperature, which varies from point to point on the impingement surface. In refs. [11, 13, 21] adiabatic wall temperature is used in calculating the heat transfer coefficient with an impinging single round jet in the presence of a cross-flowing air stream. Hollworth and Wilson [23] report measurements of effectiveness (essentially recovery factor—dimensionless adiabatic wall temperature) with an impinging circular air jet. In the same experimental apparatus Hollworth and Gero [24] investigated local heat transfer. Obot *et al.* [19] studied the effect of jet-exit geometry on impingement heat transfer. They found the jet-exit geometry mainly influences the heat transfer coefficient in the stagnation region for $L/D < 6$.

In the present investigation, adiabatic wall temperature and local heat transfer from an impinging plate to a circular air jet are measured for jet to impingement plate spacings (L/D) of 2, 4, 5, 6, 7, 8, 10 and 12, with nominal jet Reynolds numbers of 61 000, 79 000, 89 000, 106 000 and 124 000.

* Present address: University of Cincinnati, Cincinnati, OH, U.S.A.

† Present address: Control Data Corporation, Arden Hills, MN, U.S.A.

2. EXPERIMENTAL APPARATUS AND OPERATIONAL PROCEDURE

The experimental apparatus is similar to those described in refs. [11, 13, 21]; only a brief description of it is given here. The heat transfer test plate is 24.05 cm wide and 114 cm long. Air for the jet is supplied by the building compressor. After filtering and regulation, the air is metered by a replaceable thin-plate orifice. In a 127-cm-long section, an electric heater helps control the desired (total) air temperature, usually close to the ambient room air temperature. Next, the air is introduced into an insulated delivery tube 4.09 cm I.D. and 83 cm long. Attached to this tube is the jet exit assembly.

The jet exit assembly, Fig. 1a, consists of an upper bracket, a spacer and a nozzle. The upper bracket is fastened to the delivery pipe from above and a 2.54 cm thick piece of plexiglas support from below. Brass spacers of different lengths are used to vary the jet nozzle to impingement-plate spacing. The spacer is threaded into the upper bracket. The quarter-ellipse aluminum jet nozzle is designed according to the ASME power code [27]. The impinegment plate is made of thin textolite with styrofoam backing (Fig. 1b). Twenty-one stainless-steel heating foils (0.0254 mm thick) are bonded on the textolite, and 63 36-gauge iron–constantan thermocouples are embedded in the test plate in thermal contact with the stainless-steel heating foils via copper oxide.

In each test run, the mass flow is adjusted to give the desired Reynolds number and the air is heated so that:

$$T_j^\circ \simeq T_R.$$

Each test run is composed of two parts. First, the temperature distribution on the test plate is measured when the wall-heat flux is zero. This provides the adiabatic wall temperature T_{aw}. Then, the wall temperature distribution is measured on the test plate

NOMENCLATURE

A_j	jet exit area
c_p	specific heat of fluid
D	jet diameter (1.27 cm)
h	local heat transfer coefficient, $q/(T_w - T_{aw})$
$\overline{h_q}$	area average heat transfer coefficient for constant heat flux wall, $q/(\overline{T_w - T_{aw}})$
j	exponent in equation (4)
k	thermal conductivity of fluid
L	jet to impingement plate spacing
$\dot{m}_j$	jet mass flow rate
Nu	local Nusselt number, hD/k
$\overline{Nu}$	Nusselt number averaged over area from $R = 0$ to $R = R_i$ [equation (4)]
$\overline{Nu_q}$	area averaged Nusselt number for constant heat flux [equation (7)]
q	wall heat flux
Re	jet Reynolds number, $\overline{U_j}D/\nu_j$
r	recovery factor, $(T_{aw} - T_j^s)/[\bar{U}^2/(2c_p)]$
R	radial distance from geometrical center of jet—shown as greater or less than zero on the measurement line
T_{aw}	adiabatic wall temperature
T_j^s	jet static temperature
T_j°	jet total temperature, measured 127 mm upstream of the jet exit
T_R	room temperature
T_w	wall temperature
$\overline{U_j}$	jet velocity, $\dot{m}_j/\rho_j A_j$

Greek symbols

ν	kinematic viscosity
ρ_j	fluid density at jet exit.

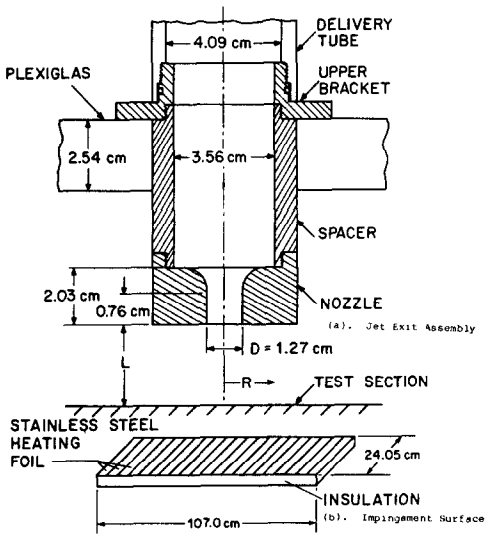

FIG. 1. Jet nozzle and test plate.

after the current is turned on in the heating foils. Approximately 1.5 h are required to reach steady-state conditions for each part of the test run.

3. RESULTS

Experimental results for heat transfer are presented in terms of the Nusselt number

$$Nu = \frac{hD}{k}. \tag{1}$$

The local heat transfer coefficient is defined by

$$h = \frac{q}{T_w - T_{aw}} \tag{2}$$

where q is the heat flux from the surface corrected for lateral conduction, for conduction to the back and for radiation. The definition of local heat transfer coefficient [equation (2)], based on the difference between the wall temperature and the adiabatic wall temperature, is well established [3, 11, 13, 21, 24]. Knowledge of T_{aw} is of great importance if meaningful results are to be obtained that can be used in different applications.

The adiabatic wall temperature measurements are presented in dimensionless form using a recovery factor

$$r = \frac{T_{aw} - T_j^s}{\bar{U}_j^2/2c_p}. \tag{3}$$

Figures 2 and 3 show the radial variation of the recovery factor for jet to impingement plate spacings (L/D) of 2 and 8, respectively. Although care was taken to set T_j° equal to the room temperature, T_R, by heating the jet air, small variations in temperature with time produced some scatter in r at low jet Reynolds number. Figures 2 and 3 each contain four graphs

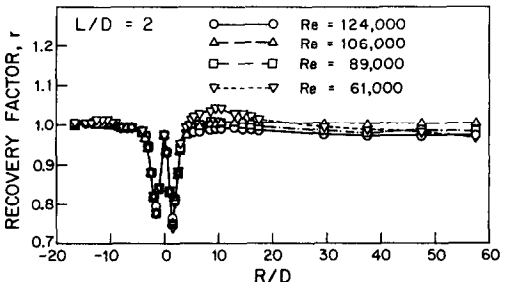

FIG. 2. Radial distribution of the recovery factor for $L/D = 2$.

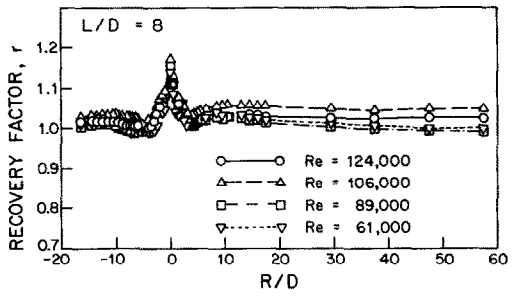

FIG. 3. Radial distribution of the recovery factor for $L/D = 8$.

corresponding to the different Reynolds numbers. Inspection of these figures and results for the other values of L/D show that the recovery factor is independent of Reynolds number. Figure 4 presents radial distributions of the recovery factor for a number of different spacings at $Re = 124\,000$. Note that r is dependent on spacing.

Figure 5 shows recovery factor as a function of L/D for various Re at $R/D = 0$ and 2. At the stagnation point ($R = 0$), for all Re the recovery factor is close to unity at $L/D = 2$, increases till $L/D \simeq 8$, and then levels off at larger spacings. For $R/D = 2$, close to the minima* shown in Fig. 2, the recovery factor is also essentially independent of Re but varies significantly with spacing. The increase in recovery factor with L/D is attributed to greater mixing of warmer ambient air (the jet static temperature is reduced below the ambient temperature by the dynamic temperature) with the jet as L/D increases.

Turning our attention back to Figs. 2–4, outside the region near stagnation (for $R/D \geqslant 4$), r is close to unity. Local minima appear near the stagnation point at $R/D \simeq \pm 2$. These local minima have their lowest value at $L/D \simeq 2$. The occurrence of significant local minima in r at small L/D can be attributed to energy separation in the highly curved flow present. At small spacing where the impingement plate would be within the potential core of the jet, the jet is surrounded by vortex rings in the shear layer. These vortex rings keep their orderly structure after impingement [28]. For vortex motion, as discussed by Hartnett and Eckert [29], an energy separation exists where the minimum energy occurs at the center of the vortex. This corresponds to the local minimum in recovery factor at $R/D \simeq 2$. At $L/D > 4$, breakdown of the vortex rings takes place [28] and the local minimum of r tends to disappear (cf. Fig. 4).

The heat transfer results are represented in dimensionless form by the Nusselt number. In general, the local Nusselt number would be a function of L/D, R/D, Pr (approximately constant in the present study)

* As measurements were taken along a line through the stagnation point on the plate, values of R greater and less than zero are plotted. Since the jet is axisymmetric this is not strictly necessary. The minima discussed at $R/D \simeq \pm 2$ are really one off-center minimum.

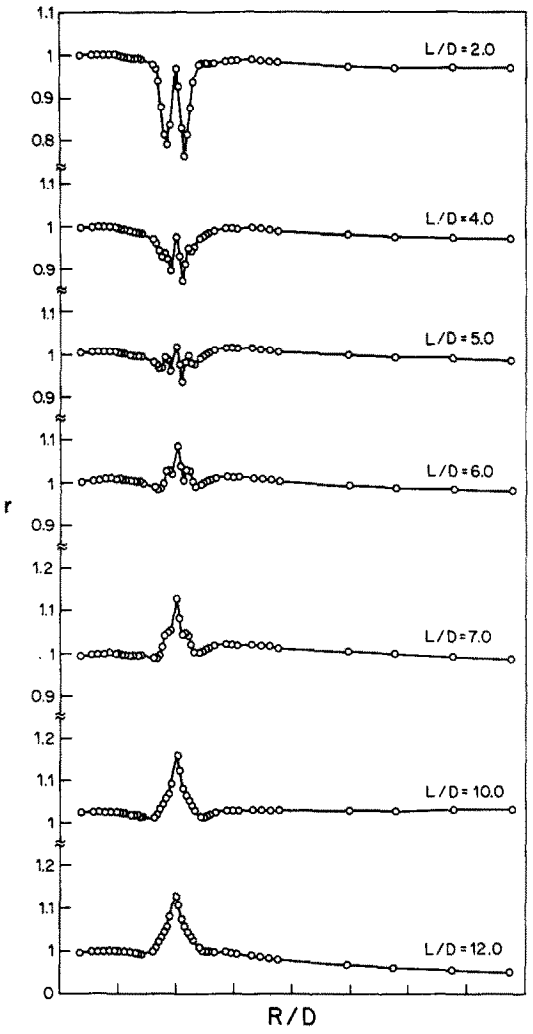

FIG. 4. Radial distribution of the recovery factor at different jet to plate spacings, $Re_j \simeq 124\,000$.

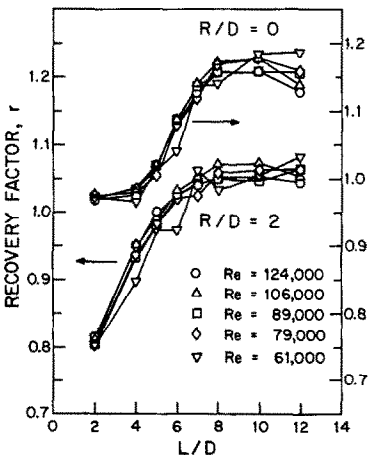

FIG. 5. Variation of the recovery factor with jet to impingement plate spacing at $R/D = 0$ and 2.0.

Table 1.

Ref.	Author(s)	Geometry	D (cm)	$Re_j = U_jD/D$	L/D	Type of measurements	Fluid outlet
1	Perry	long nozzle, length not known at angles	1.65, 2.16	7×10^3–30×10^3 for $D = 1.65$	$\geqslant 8$	area average	hot air in all directions
2	Vikers	short tube, length not known	not known	250–950	$8 \leqslant L/D \geqslant 20$	local	air into a circular box in all directions
3	Gardon and Cobonpue	well rounded inlet and short throat, length not known	0.23–0.9	7×10^3–1.12×10^5	$\geqslant 0.5$	local	air in all directions
4	Smirnov *et al.*	long tube, length = $80D$	0.25, 0.64, 1.07, 2.13, 3.0, 3.66	50–31×10^3	$0.5 < L/D > 10$	averaged	water in all directions
5	Huang	orifice thickness = $0.317D$	0.317, 0.635	10^3–10^4	1.25–10	averaged (2.5 cm) around-stagnation	hot air in all directions
6	Schlunder and Gnielinski	long tube, length not known	2, 5	34×10^3 · 124×10^3	1.25–10	local mass transfer	air in all directions
7	Nakatogawa *et al.*	nozzle	0.8	area average velocity = 35–321 m s^{-1}	0.5–24	around stagnation	all directions
8	Kataoka and Mizushina	convergent nozzle	1	2970, 5030, 9800	5.86, 8.21	mass transfer	electrochemical technique
9	Donaldson and Snedeker	convergent nozzle	1.29	based on half radius	7, 10, 15, 20,20	mass transfer	air in all directions
10	Den Ouden and Hogendoorn	nozzle	1.3–5.7	0.38×10^5–2.64×10^5	1–6	local around stagnation	air in all directions
11	Bouchez and Goldstein	orifice $L/D = 12$, tube $L/D = 6$	1.27	35×10^3 125×10^3	6, 12	local	air impingement in a well-defined crossflow

12	Hollworth and Bowley	nozzle $10D$ long, orifice $1/D$ long	0.318–1.27	2.5×10^4 1.9×10^5	3.5–14	local	air impingement in a well-defined crossflow
13	Sparrow *et al.*	orifice for $L/D = 12$ or various lengths for $3 \leqslant L/D$ 12	1.27	35×10^3 125×10^3	3, 4, 5, 6, 8, 10, 12	local	air impingement in a well-defined crossflow
14	Hoogendoorn	long tube and nozzle with smooth contraction	5.7	2×10^4–9×10^4	2–10	local liquid crystal	air in all directions
15	Kataoka *et al.*	nozzle smooth contraction	2.8	4×10^3–15×10^3	2–10	local mass transfer	electrochemical technique
16	Yokobori and Hirata	nozzle	4.0	10^3–67×10^3	2–12	local around stagnation	water flow visualization
17	Popiel *et al.*	exit of tunnel burner	1.38	1860–1050	2–20	local heat flux meter	combustion products in all directions
18	Sparrow and Lovell	orifice at angles 90°–30°	0.635	2.5×10^3–10^4	7, 10, 15	local mass transfer (napthlene)	air in all directions
19	Obot *et al.*	orifice of various thicknesses and rounded nozzle of various lengths	1.905	15×10^3–60×10^3	2–12	local	air in all directions
20	Amano and Jensen	not clear exp. and num.	0.46	10^4–2×10^4, 4×10^4	4, 7, 10	local	air in all directions inside large enclosure
21	Goldstein and Behbahani	orifice, $L/D = 12$, tube $L/D = 6$	1.27	25×10^3 124×10^3	6, 12	local	air with and without crossflow
22	Goldstein and Timmers	orifice thickness $= D$	1.00	40×10^3	2, 6	local (liquid crystals)	air in all directions
23	Hollworth and Wilson	orifice thickness $= D$	0.25, 1.0	7×10^3–7×10^4	1, 5, 10, 15	local	air in all directions
24	Hollworth and Gero	orifice thickness $= D$	0.25, 1.0	5×10^3–6×10^4	1, 5, 10, 15	local	air in all directions
25	Hrycak	orifice at the end of a tube	0.318–1.27	1.4×10^3–6×10^4	1–14	average over area of 5 mm diameter	air in all directions
	Present study	orifice	1.27	61×10^3–12×10^4	2–12	local	air in all directions

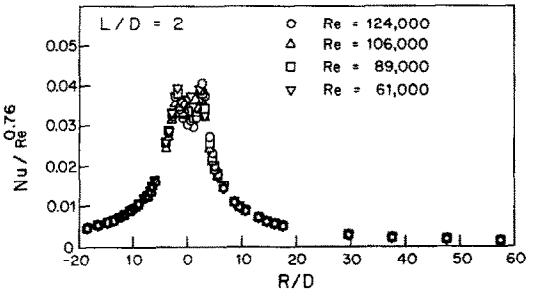

FIG. 6. Radial distribution of $Nu/Re^{0.76}$ for $L/D = 2$.

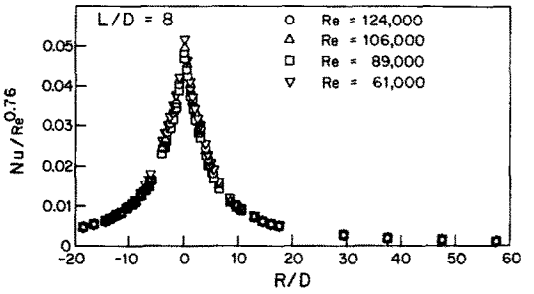

FIG. 8. Radial distribution of $Nu/Re^{0.76}$ for $L/D = 8$.

and Re. The dependence on Re can be approximated by a power-law dependence

$$Nu \propto Re^{j}. \tag{4}$$

The value of j is somewhat dependent on R/D. Close to the stagnation point j is smaller (~ 0.5 for small L/D) than at larger R. For a plane wall jet, values of 0.75(30) and 0.80(31) have been found. For convenience, a constant value of j is used in the present correlation (cf. discussion on correlation below).

Figures 6–9 contain plots of $Nu/Re^{0.76}$ as a function of radial position for jet to impingement plate spacings (L/D) of 2, 5, 8 and 10 respectively. On each figure, results for $Re = 61\,000$, 89 000, 106 000 and 124 000 are presented. As can be seen from these figures, $Nu/Re^{0.76}$ is essentially independent of Re for all L/D in the range of the present experiments except close to $R = 0$. $Nu/Re^{0.76}$ has little dependence on L/D as well as Re in regions for which $|R/D| \geqslant 4$. At these large radii Nu decreases as a result of the increase in the boundary thickness.

In the stagnation region, Nu varies with spacing. At small spacing ($L/D = 2$, 4 and 5), secondary maxima appear at $R/D \simeq \pm 2$. For $L/D = 2$, these local maxima are higher than the stagnation ($R/D = 0$) values of Nu (Fig. 6). This can also be observed in Fig. 10, where $Nu/Re^{0.76}$ is shown as a function of L/D for the different Re at $R/D = 0$ and 2. The local maxima at $R/D \simeq 2$ are attributed to the enhancement of heat transfer from entrainment caused by vortex rings in the shear layer. Local maxima in Nu were also observed by other investigators [3, 14, 22]. The stagnation Nu increases with L/D and reaches its maximum at $L/D = 8$, beyond which it decreases (cf. Fig. 10). This increase in stagnation Nu can be related to penetration of turbulent-induced mixing from the shear layer. The decrease beyond $L/D = 8$ is a consequence of lower arrival velocity of the jet. Note again there is little effect of spacing on Nu for $R/D > 4$ in the range of the present tests.

As the jet is axisymmetric, the radial distribution of Nu can be averaged to give the mean Nusselt number

$$\overline{Nu} = \frac{2}{R^2}\int_0^R NuR\,\mathrm{d}R. \tag{5}$$

The integral is determined numerically for $R/D = 0.5$, 1, 2, 3, 6, 18 and 32 for $L/D \geqslant 6$. These results are satisfactorily correlated by:

$$\frac{\overline{Nu}}{Re^{0.76}} = \frac{(A - |L/D - 7.75|)}{B + C(R/D)^n} \tag{6}$$

where $A = 24$, $B = 533$, $C = 44$ and $n = 1.285$. Figure 11 shows this correlation; the spread in the data is indicated by the vertical bars.

Equation (5) evaluates $\overline{Nu}$ based on the assumption of constant $(T_w - T_{aw})$ over the impingement surface. In this study, however, heat flux at the wall is constant. Defining an average temperature difference

$$\overline{T_w - T_{aw}} = \frac{2}{R^2}\int_0^R (T_w - T_{aw})R\,\mathrm{d}R \tag{7}$$

and

$$\overline{h_q} = q/(\overline{T_w - T_{aw}}) \tag{8}$$

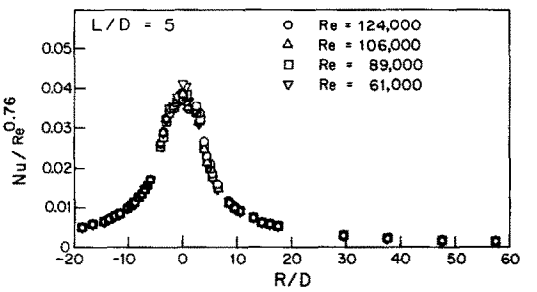

FIG. 7. Radial distribution of $Nu/Re^{0.76}$ for $L/D = 5$.

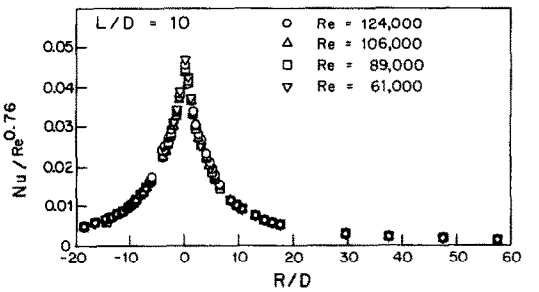

FIG. 9. Radial distribution of $Nu/Re^{0.76}$ for $L/D = 10$.

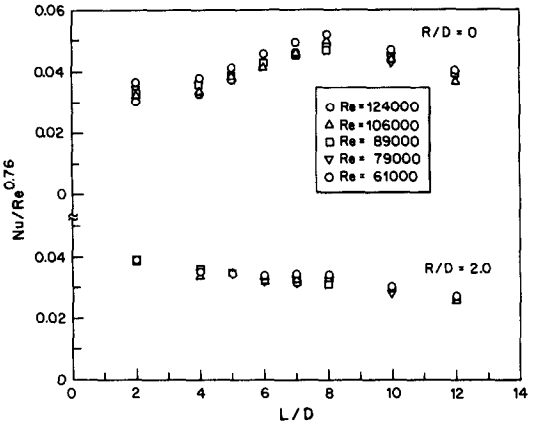

FIG. 10. Variation of $Nu/Re^{0.76}$ with jet to impingement plate spacing at $R/D = 0$ and 2.0.

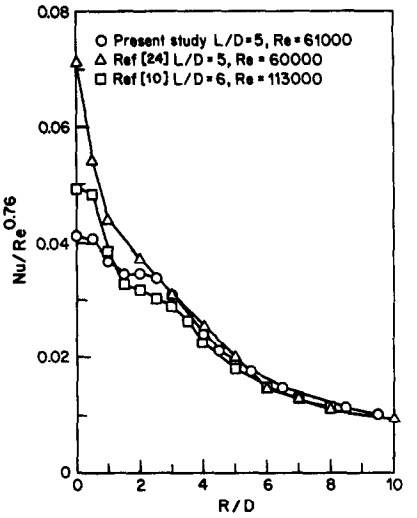

FIG. 12. Comparison of the local heat transfer results with other studies.

the area-averaged Nusselt number based on the constant heat flux becomes:

$$\overline{Nu_q} = \frac{R^2}{2} 1 \Big/ \int_0^R \frac{1}{\overline{Nu}} R \, dR. \tag{9}$$

A correlation similar to equation (6) can be obtained to describe $\overline{Nu_q}$

$$\frac{\overline{Nu_q}}{Re^{0.76}} = \frac{(A - |L/D - 7.75|)}{B + C(R/D)^m} \tag{10}$$

where A, B and C are as given for equation (6) above and $m = 1.394$. The range of validity is the same as for equation (6). $\overline{Nu_q}$ is found to be closely equal to $\overline{Nu}$ (cf. Fig. 11) up to $R/D = 4$. At larger R/D, $\overline{Nu_q}$ is somewhat higher than $\overline{Nu}$.

The exponent, 0.76, for equations (4) and (10) is chosen from a least-squares analysis to minimize the standard deviation of the data from the correlation. The variation of the standard deviation with the value of the exponent is small in the region of the minimum, and other values could be used. If 0.75 or 0.8 were used for j, equations (6) and (9) would be little changed other than $A = 475$ and $B = 39$ when $j = 0.75$ and $A = 842$ and $B = 70$ when $j = 0.8$. These variations in the correlation have some merit when comparing the results to analytical predictions particularly in the wall jet region at large R.

Comparison of results

Local heat transfer results are compared in Fig. 12 with results from earlier investigations. Inspection of Fig. 12 shows good agreement between the present study and those of refs. [10, 24] for $R/D > 2$. However, considerable differences in heat transfer coefficients exist in the stagnation region ($R/D < 2$). This discrepancy can be attributed [19], at least partly, to differences in the jet-exit geometries of the different studies. Area averaged heat transfer coefficients are compared in Table 2 with the correlation in ref. [26] using results of various investigators. Good agreement is observed.

4. SUMMARY AND CONCLUDING REMARKS

The recovery factor on the impingement surface is independent of jet Reynolds numbers, but is dependent on jet to impingement plate spacing. At small

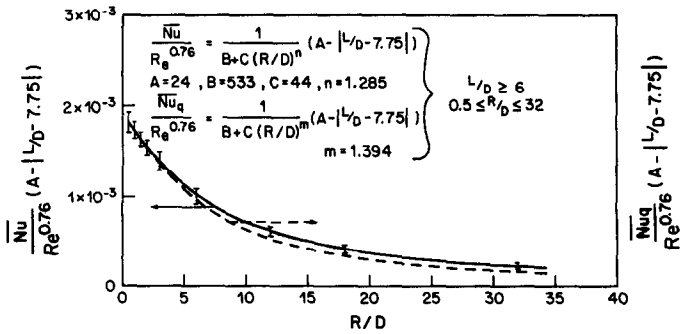

FIG. 11. Area-averaged heat transfer correlation for constant surface heat flux and constant surface temperature.

Table 2. Comparison of area-averaged Nusselt number

		$Re = 61\,000$		$Re = 89\,000$		$Re = 12\,400$	
			Present study		Present study		Present study
R/D	L/D	Ref. [26]	$\overline{Nu_q}$	*Ref.* [26]	$\overline{Nu_q}$	Ref. [26]	$\overline{Nu_q}$
3	6	159	151	207	202	261	260
	8	149	162	194	216	245	278
	12	133	134	172	179	218	231
6	6	103	126	133	168	168	217
	8	99	134	129	180	163	232
	12	93	112	121	150	153	193

spacing, the recovery factor in the stagnation region has a minimum near $R/D \simeq 2$ apparently due to energy separation in the vortex ring region in the shear layer. For L/D greater than about 5 up to the largest spacing studied ($L/D = 12$), the stagnation region recovery factor can be greater than unity due to mixing of the ambient fluid with the jet. The heat transfer is best correlated by $Nu/Re^{0.76}$ for all L/D. The Nusselt number has a maximum at $R/D \simeq 2$ for jet-to-plate spacings up to $L/D = 5$. The maximum stagnation Nusselt number occurs at about $L/D = 8$.

Acknowledgement—The research was supported by a grant from the Engineering Research Program of the Office of Basic Energy Science, U.S. Department of Energy.

REFERENCES

1. K. P. Perry, Heat transfer by convection from a hot gas jet to a plane surface, *Proc. mech. Engng Inst.* **168,** 775–784 (1954).
2. J. M. F. Vikers, Heat transfer coefficients between fluid jets and normal surfaces, *Ind. Engng Chem.* **51,** 967–972 (1959).
3. R. Gardon and J. Cobonpue, Heat transfer between a flat plate and jets of air impinging on it, *Int. Developments in Heat Transfer, Proc. 2nd Int. Heat Transfer Conference*, pp. 454–460. ASME, New York (1962).
4. V. A. Smirnov, G. E. Verevochkin and P. M. Brdlick, Heat transfer between a jet and a held plate normal to the flow, *Int. J. Heat Mass Transfer* **2,** 1–7 (1961).
5. G. C. Huang, Investigations of heat transfer coefficients for air flow through round jets impinging normal to a heat transfer surface, ASME paper No. 62-HT-31 (1962).
6. E. U. Schlunder and V. Gnielinski, Warme- und Stoffubertrasuns zwischen Gut und aufprallendern Dusenstrahl, *Chemie-Ingr-Tech.* **39,** 578–584 (1967).
7. T. Nakatogawa, N. Nishiwaki, M. Hirata and K. Torii, Heat transfer of round turbulent jet impinging normally on flat plate, *Proc. 4th Int. Heat Transfer Conference*, Vol. II, FC5.2, edited by U. Grigull (1972).
8. K. Kataoka and T. Mizushina, Local enhancement of the rate of heat transfer in an impinging round jet by free-stream turbulence, *Proc. 4th Int. Heat Transfer Conference*, Vol. II. pp. 305–309. Japanese Societies of Mechanical and Chemical Engineers (1974).
9. C. D. Donaldson and M. Snedeker, A study of free jet impingement, Part II, free jet turbulent structure and impingement heat transfer, *J. Fluid Mech.* **45,** 477–512 (1971).
10. C. den Ouden and C. J. Hoogendoorn, Local convective heat transfer coefficients for jets impinging on a plate; experiments using a liquid-crystal technique, *Proc. 5th Int. Heat Transfer Conference*, Vol. 5, pp. 293–297. Japanese Societies of Mechanical and Chemical Engineers (1974).
11. J. P. Bouchez and R. J. Goldstein, Impingement cooling from a circular jet in a crossflow, *Int. J. Heat Mass Transfer* **18,** 719–730 (1975).
12. B. R. Hollworth and W. W. Bowley, Heat transfer characteristics of an impinging jet in a crossflow, ASME paper No. 75-WA/HT-100 (1975).
13. E. M. Sparrow, R. J. Goldstein and M. A. Rouf, Effect of nozzle surface separation distance on impingement heat transfer for a jet in a crossflow, *J. Heat Transfer* **97,** 528–533 (1975).
14. C. J. Hoogendoorn, The effect of turbulence on heat transfer at a stagnation point, *Int. J. Heat Mass Transfer* **20,** 1333–1338 (1977).
15. K. Kataoka, T. Komai and G. Nakamura, Enhancement mechanism of mass transfer in a turbulent impinging jet for high Schmidt numbers, ASME paper No. 78-HT-5 (1978).
16. K. Yokobori, N. Kasagi and M. Hirata, Characteristic behavior of turbulence and transport phenomena at the stagnation region of an axisymmetric impinging jet, 2nd Symposium on Turbulent Shear Flows, Imperial College, London (July 1979).
17. C. O. Popiel, T. H. van deer Meer and C. J. Hoogendorn, Convective heat transfer on a plate in an impinging round hot gas jet of low Reynolds number, *Int. J. Heat Mass Transfer* **23,** 1055–1068 (1980).
18. E. M. Sparrow and B. J. Lovell, Heat transfer characteristics of an obliquely impinging circular jet, *J. Heat Transfer* **102,** 202–209 (1980).
19. N. T. Obot, A. S. Majumdar and W. J. M. Douglas, The effect of nozzle geometry on impingement heat transfer under a round turbulent jet, ASME paper No. 79-WA/HT-53 (1979).
20. R. S. Amano and M. K. Jensen, A numerical and experimental investigation of turbulent heat transport of an axisymmetric jet impinging on a flat plate, ASME paper No. 82-WA/HT-55 (1982).
21. R. J. Goldstein and A. I. Behbahani, Impingement of a circular jet with and without cross flow, *Int. J. Heat Mass Transfer* **25,** 1377–1382 (1982).
22. R. J. Goldstein and J. F. Timmers, Flow visualization of impinging jets, *Int. J. Heat Mass Transfer* **25,** 1857–1868 (1982).
23. B. R. Hollworth and S. I. Wilson, Entrainment effects on impingement heat transfer. Part I: measurement of heated jet velocity and temperature distribution, and recovery temperature on target surface, ASME paper No. 83-HT-8 (1983).
24. B. R. Hollworth and L. R. Gero, Entrainment effects on impingement heat transfer. Part II: local heat transfer measurements, ASME paper No. 84-HT-20 (1984).

25. P. Hryack, Heat transfer from round impinging jets to a flat plate, *Int. J. Heat Mass Transfer* **26**, 1857–1865 (1983).
26. H. Martin, Heat and mass transfer between impinging gas jets and solid surfaces. In *Advances in Heat Transfer* (Edited by T. Irvine and J. P. Hartnett), Vol. 13, pp. 1–60. Academic Press, New York (1977).
27. *Fluid Meter, the Theory and Application*, Report of ASME Research Committee on Fluid Meters ASME, New York, pp. 46–47 (1959).
28. S. Yokobori, N. Kasagi, M. Hirata, M. Nakamaru and K. Haramura, Characteristic behavior of turbulence and transport phenomena at the stagnation region of an axisymmetrical impinging jet. Presented at the 2nd Symposium on Turbulent Shear Flows, Imperial College, London (July 1979).
29. J. P. Hartnett and E. R. G. Eckert, Experimental study of the velocity and temperature distribution in a high velocity vortex-type flow, *Trans. Am. Soc. mech. Engrs* **79**, 751–758 (1957).
30. R. A. Seban and L. H. Back, Velocity and temperature profiles in a wall jet, *Int. J. Heat Mass Transfer* **3**, 255–265 (1961).
31. G. E. Myers, J. J. Schauer and R. H. Eustis, Heat transfer to plane turbulent wall jets, *J. Heat Transfer* **85**, 209–214 (1963).

DISTRIBUTION DU FACTEUR DE RECUPERATION ET DU COEFFICIENT LOCAL DE CONVECTION POUR UN JET D'AIR CIRCULAIRE IMPACTANT

Résumé—On décrit une étude de la distribution radiale du facteur de récupération et du coefficient de convection local pour un jet axisymétrique d'air qui sort d'une tuyère lisse et qui frappe une surface. Le facteur de récupération dépend de la distance entre la sortie du jet et la plaque, mais il est indépendant du nombre de Reynolds. Le maximum du transfert thermique au point d'arrêt est obtenu à une distance de huit diamètres. Une formule est donnée pour le transfert thermique global sur la surface.

VERTEILUNG DES 'RECOVERY'-FAKTORS UND DES ÖRTLICHEN WÄRMEÜBERGANGSKOEFFIZIENTEN BEIM AUFTREFFEN EINES LUFTSTRAHLES MIT KREISQUERSCHNITT

Zusammenfassung—Beschrieben wird eine Untersuchung der radialen Verteilung des 'Recovery'-Faktors und des örtlichen Wärmeübergangskoeffizienten beim Auftreffen eines axialsymmetrischen Luftstrahles, der durch eine gut gerundete Düse erzeugt wird. Der 'Recovery'-Faktor ist abhängig vom Abstand zwischen der Düse und der angeströmten Platte, jedoch unabhängig von der Reynoldszahl des Strahles. Der maximale Wärmeübergangskoeffizient im Staugebiet ergibt sich, wenn der Düsenabstand dem achtfachen Strahldurchmesser entspricht. Es wurde eine Beziehung für den mittleren Wärmeübergangskoeffizienten an der Oberfläche ermittelt.

РАСПРЕДЕЛЕНИЕ В РАДИАЛЬНОМ НАПРАВЛЕНИИ КОЭФФИЦИЕНТОВ ВОССТАНОВЛЕНИЯ И ЛОКАЛЬНОГО ТЕПЛОПЕРЕНОСА К КРУГЛОЙ ВОЗДУШНОЙ СТРУЕ, НАТЕКАЮЩЕЙ НА ПРЕГРАДУ

Аннотация—Описываются результаты исследования радиального распределения коэффициента восстановления и локального теплопереноса для осесимметричной набегающей струи воздуха, истекающей из гладкого сопла. Показано, что коэффициент восстановления зависит от отношения расстояния до пластины к диаметру сопла, но независим от числа Рейнольдса струи. Максимальная застойная область теплообмена имеет место при указанном геометрическом соотношении, равном 8. Получена зависимость для осредненного теплопереноса с поверхности.